

Modelling and optimization of compact subsea liquid-liquid separation system

Tamal Das^a, Preben Først Tyvold^a and Johannes Jäschke^{a,*}

^a*Norwegian University of Science and Technology, Kjemiblokk 4, Trondheim N-7034, Norway*

**jaschke@ntnu.no*

Abstract

Subsea separation systems require compactly sized separators because they are easier to install on the sea bed and require less material of construction to withstand high pressures subsea. The compactness of the separators is brought about by using cyclonic forces, which are many times stronger than gravitational force to drive separation. Existing models are typically intended for design purposes, but they are computationally intensive and are not suitable to be used in numerical optimization methods. Hence, in this work, we developed a simple, yet reasonably accurate model for a subsea separation system, in which the oil-water emulsion feed undergoes a preliminary bulk separation in a gravity separator into two crudely separated streams. A further purification is carried out for the oil-rich stream in a dewaterer and the water-rich stream in a deoiler. Our models calculate the oil cut in the outgoing streams based on separator design and operational parameters, such as flow split, feed flow rate, and oil cut of the incoming stream. The deoiler model was calibrated using data from literature and the system was used for optimization to maximize the oil cut in the oil-rich product using the flow splits of the individual separators as degrees of freedom. The model was used to study the optimal flow splits corresponding to different feed rates and inlet oil cuts.

Keywords: compact separator, modelling, optimization, subsea processing

1. Introduction

Subsea processing of hydrocarbons can offer significant reduction in operating costs and capital costs and can prolong hydrocarbon production from low pressure reservoirs. Hence, it not only results in higher economic value, but also enables production from wells that are otherwise economically infeasible to extract from. However, the subsea facilities, being compact, are challenging to control due to short residence time of fluids within them. To be able to study and operate such systems optimally, a good model of the system is required. These models can provide results that are reliable and easy to interpret, which empirical models fail to provide. In the past decade, several attempts have been made to understand oil-water separation. Slot (2013) modelled swirl separators for design purposes, while van Campen (2014) investigated droplet dynamics inside liquid-liquid axial cyclones. Sayda and Taylor (2007) provided a dynamic model for liquid-liquid separation in a continuous water-continuous gravity separator. In this work, we developed a system of simplified steady state models of separators to study optimal operation. We calibrate our deoiler model against experimental results provided by van Campen (2014).

2. Process description

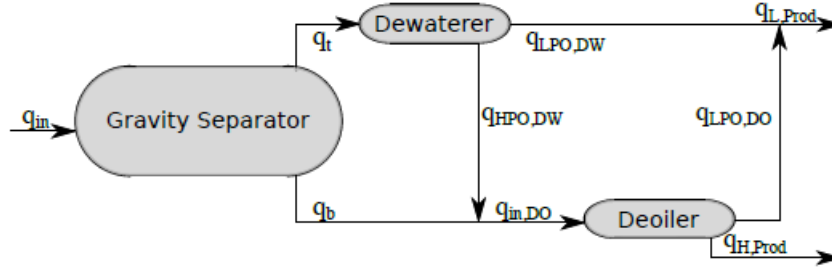


Figure 1: The separation system

Figure 1 shows the overall separation system with the flow connections. The outlets from the gravity separator (G) q_t and q_b are the top and the bottom flows, respectively. The top flow q_t is likely to be rich in oil and needs to be treated further to remove the residual water in it. Hence, this stream is fed to the dewaterer (DW). The LPO stream out of the dewaterer is oil-rich and combines with the oil-rich LPO stream out of the deoiler (DO) to give the final oil product. The HPO stream out of the dewaterer that is rich in water combines with the water-rich stream out of the gravity separator and is fed into the deoiler for the removal of the residual oil. The water rich HPO stream out of the deoiler is the separated water out of the system.

The fluid properties used in the model are chosen in order to reconstruct the oil phase and the water phase used in the experiments conducted by van Campen (2014). To imitate the subsea scenario, brine is considered as the water phase. The densities and viscosities of the two phases are given in Table 1.

Table 1: Properties of the oil and the brine used in the models

Liquid	Density [kg/m^3]	Viscosity [$mPa.s$]
Oil	881	8.8
Brine	1064	1.0

3. Models

Liquid-liquid systems typically exist as emulsions made of a continuous phase and a dispersed phase. In case of oil-water systems, oil is usually the lighter of the two phases. An oil continuous system is called water-in-oil system (WiO) because the water phase exists as the dispersed phase, while a water continuous system is called oil-in-water system (OiW) consisting of oil as the dispersed phase. Due to the difference in densities of the two phases, water sediments in WiO systems or oil creams in OiW systems. The movement of the dispersed phase in emulsions can be approximately assumed to be described by the following terminal velocity expression given by Stokes' law, where r_d is the droplet radius of the dispersed phase, g is the acceleration due to gravity, $(\rho_d - \rho)$ is the difference in densities of dispersed phase and the continuous phase and μ is the viscosity of the fluid.

$$v = \frac{2r_d^2(\rho_d - \rho)g}{9\mu} \quad (1)$$

The viscosity of the emulsion is a function of the oil cut expressed as a third order polynomial in Table 2. The polynomial function has been fitted to the values measured by van Campen (2014). The emulsion undergoes a phase inversion from OiW to WiO at an oil cut of about 0.66. Hence,

there are two polynomial fits, one representing oil cuts lower than 0.66 and the other representing oil cuts higher than 0.66 or water cuts lower than 0.34. The coefficients of the polynomial fits are given in Table 2.

Table 2: Coefficients in the polynomial for viscosity of emulsion $\mu = \mu_c(1 + a\phi + b\phi^2 + c\phi^3)$, where μ_c is the viscosity of continuous phase and ϕ is the volume fraction of the dispersed phase

Emulsion	ϕ [-]	a [-]	b [-]	c [-]
Oil-in-water	0 - 0.66	110	-400	470
Water-in-oil	0 - 0.34	-1.6	27	23

3.1. Simplified models for inline cyclonic separators

All cyclonic separators considered in this paper are cylindrical in shape with one axial input and two axial outlets. The inlet conditions and the dimensions of the separators are given in the Table 3. The strength of the swirl element is represented by swirl number Ω , which is further used in the model equations.

Table 3: Dimensions of the inline cyclonic separators

Length	Outer pipe	Deoiler inner pipe	Dewaterer inner pipe	Swirl number
L [m]	R [m]	R_i [m]	R_i [m]	Ω [-], large / strong / weak
1.7	0.05	0.025	0.043	7.0 / 5.0 / 3.5

The cyclonic separators, i.e. deoiler and dewaterer have been modelled in the same way. We present the deoiler model here. The model for dewaterer is analogous to that of the deoiler with an essential difference that the dispersed phase is water instead of oil. The deoiler has an axial inlet and two outlets. The outlet close to the axial center having a circular cross-section with radius R_i is called the light phase outlet (LPO) and the associated flow rate is denoted by q_{LPO} . The other outlet having an annular cross-section that starts at radius R_i and ends at the separator radius R is called the heavy phase outlet (HPO) and the associated flow rate is denoted by q_{HPO} . The flow inside the separator is assumed to be consisting of two plug flows corresponding to the two outflows, the velocities of which are given by Equation 2.

$$v_z(r) = \begin{cases} \frac{q_{LPO}}{\pi R_i^2}, & \text{if } 0 \leq r \leq R_i \\ \frac{q_{HPO}}{\pi(R^2 - R_i^2)}, & \text{if } R_i < r \leq R \end{cases} \quad (2)$$

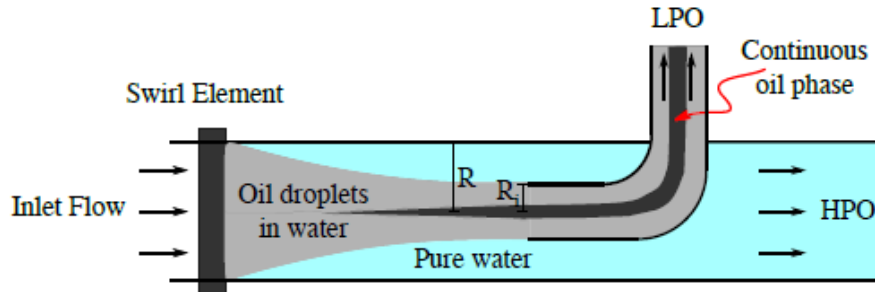


Figure 2: Flow behavior inside a cyclonic separator

The plug velocities can be changed by changing the outlet flow split (FS), which is q_{LPO}/q_{in} . When the fluid enters the separator, it encounters a swirl element that introduces a tangential component to the velocities of the fluid particles. The tangential velocity considered in this model at an axial position increases linearly from the center to a radius R_c , beyond which the velocity stays constant until the edge of the separator. The tangential velocity v_θ^0 at the inlet of the separator just after the swirl element is given by the Equation 3, where the v_θ^{max} is expressed as a product of the bulk axial velocity $v_{z,b}$ and the swirl strength Ω . R_c represents Rankine vortex and typically has a value $0.25R$, as reported by Dirkwanger (1996). The function for $v_\theta^0(r)$ is not continuously differentiable at $r = R_c$. This function has been smoothed using method by Balakrishna and Biegler (1992) to enable ease in computation while using numerical optimization solver *fmincon* in MATLAB.

$$v_\theta^0(r) = \begin{cases} v_\theta^{max} \frac{r}{R_c}, & \text{if } 0 \leq r \leq R_c \\ v_\theta^{max}, & \text{if } R_c < r \leq R \end{cases} \quad (3)$$

The tangential velocity undergoes a decay along the length of the separator due to a loss in momentum, expressed by Equation 4. The damping coefficient C_{decay} of 0.04 was reported by Dirkwanger (1996) and Slot (2013). The radial velocity v_r of the dispersed droplets is calculated using the Equation 1 and replacing the g in that expression with radial acceleration $v_\theta^2(r, z)/r$.

$$v_\theta(r, z) = v_\theta^0(r) e^{-\frac{C_{decay}z}{2R}} \quad (4)$$

The oil volume fractions in the *LPO* and *HPO* streams are given by Equation 5 and Equation 6, respectively and the oil volume fraction at any spacial location $\alpha_c(r, z)$ inside the separator is given by Equation 7, which can be derived by oil flux balance. Equation 5 assumes that all the droplets that enter the separator at radii lesser than r_{in} travel through the separator to end up in the *LPO*.

$$\alpha'_{LPO} = \alpha_{in} \frac{FS(R^2 - R_i^2) + (1 - FS)(r_{in}^2 - R_i^2)}{FS(R^2 - R_i^2)} \quad (5)$$

$$\alpha'_{HPO} = \frac{\alpha_{in} - \alpha'_{LPO}FS}{1 - FS} \quad (6)$$

$$\alpha_c(r, z) = \alpha_{in} \frac{FS(R^2 - R_i^2) + (1 - FS)(r_{in}^2 - R_i^2)}{(1 - FS)(r^2 - R_i^2) + FS(R^2 - R_i^2)} \quad (7)$$

The empirical correlation for droplet radius r_d is fitted against results by van Campen (2014).

$$r_d(v_\theta^{max}) [m] = \begin{cases} (-53.5v_\theta^{max} + 300) \cdot 10^{-6}, & v_\theta^{max} [m/s] \leq 4.45 \\ (-4v_\theta^{max} + 80) \cdot 10^{-6}, & v_\theta^{max} [m/s] > 4.45 \end{cases} \quad (8)$$

To compensate for the errors in assumption of a simplistic flow pattern, it is assumed that a re-entrainment of one flow in the other flow due to the difference in the velocities of the two plug flows is highly likely. Hence, a re-entrainment flow rate of q_{re-en} enters the *LPO* stream given by $k_{re-en}(v_{LPO} - v_{HPO})$, where parameter k_{re-en} was determined to be $2 \cdot 10^{-4} m^2$ by fitting the model to the experimental results by van Campen (2014). Accordingly, changes are made in the oil volume fraction α_{LPO} , while α_{HPO} is computed as $(\alpha_{in} - \alpha_{LPO}FS)/(1 - FS)$.

$$\alpha_{LPO} = \frac{\alpha'_{LPO}(q_{LPO} - q_{re-en}) + \alpha'_{HPO}q_{re-en}}{q_{LPO}} \quad (9)$$

We solved for the inlet radius r_{in} of the entering droplet that will exit exactly at R_i at outlet boundary. To solve this boundary value problem (BVP), the radial velocity v_r was integrated using a second order, explicit Runge-Kutta integrator with a constant time step of one-tenth of the residence time L/v_{HPO} . The BVP was solved using a *shooting method* given by Constantinides and Mostoufi (1999), which uses the Newton-Raphson method.

3.2. Simplified model for gravity separator

The gravity separator has been modelled considering mono-dispersed oil droplets. The model is a steady state adaptation of the dynamic model given by Sayda and Taylor (2007), considering two phases instead of three phases. The separator dimensions used in the model are given in Table 4. The droplets move vertically upwards travelling from the inlet of the separator to the end of the separator as shown in the Figure 3. The bottom outlet, i.e. the heavy phase outlet q_b contains the emulsion that remains un-separated under the weir height H_w . The height Δh at the end of the separator, which denotes the level of pure water phase, can be computed as Lv_v/v_h , where L , v_h , v_v are the length of the separator, the horizontal velocity and the vertical velocity of the droplets, respectively. v_h can be calculated as q_b/A_b ,

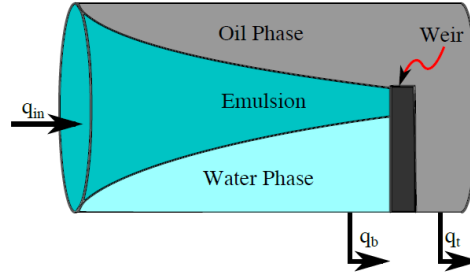


Figure 3: Dimensions of the gravity separator

Table 4: Input to the gravity separator

Length L [m]	Outer pipe R [m]	Weir height H_w [m]	Droplet diameter D_d [μm]
7	1.7	2.55	120

where A_b is the section of the circular area of the cylinder lying below the weir as shown in Figure 4. v_v is given by Equation 1. The oil volume fraction of the outlets α_b and α_t can be calculated as $\alpha_{in}A_e/A_b$ and $[\alpha_{in}q_{in} - \alpha_bq_b]/q_t$, respectively, where A_e is as shown in Figure 4.

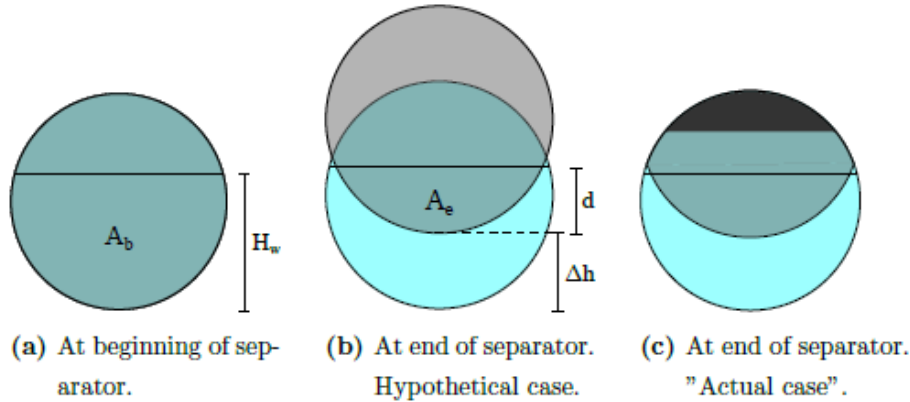


Figure 4: Cross section of gravity separator at the beginning and end of the gravity separator

4. Results

The model of separation system was used to maximize the oil volume fraction in the overall light phase outlet $q_{L,Prod}$ with a constraint of oil cut in final water-rich stream to be less than 3%. The optimizer found optimal flow splits of the three separators for several inlet oil cuts and inlet flow rates. The model for deoiler has been calibrated against experimental results from van Campen (2014).

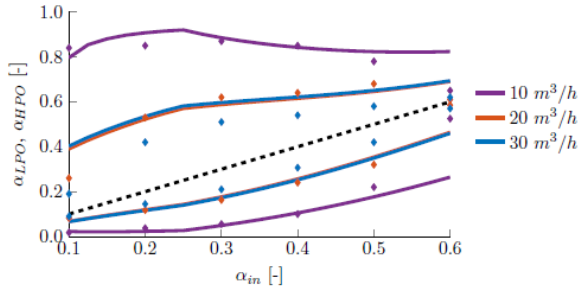


Figure 5: Oil volume fractions of the outlets vs inlets in a deoiler (experimental vs model results)

Figure 5 presents the comparison of the experimental results with the model results for different inlet oil volume fractions to the deoiler. The model was fitted for a throughput of $10 \text{ m}^3/\text{h}$. The model overpredicts the separation performance at higher throughput, and very low and very high inlet oil cuts possibly because of unaccounted effects of droplet break-up and droplet coalescence.

gravity separator rise as inlet oil cut rises because of higher oil load. Figure 7 shows optimal flow splits for changing throughput. The sign of the slope of optimal flow splits change around $20 \text{ m}^3/\text{h}$ because both the deoiler and the dewaterer reach peak separation performance at $8 \text{ m}^3/\text{h}$.

The optimization results in Figure 6 are as expected as the flow split for dewaterer falls and that for deoiler and

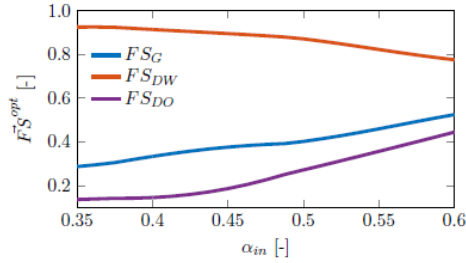


Figure 6: Optimal flow splits of separators vs inlet oil volume fraction ($q_{in} = 20 \text{ m}^3/\text{h}$)

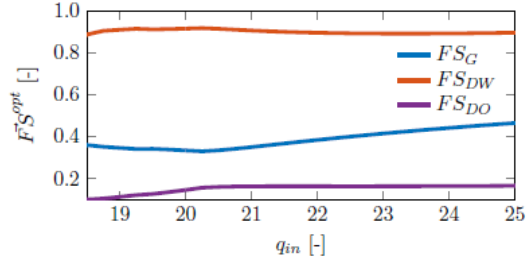


Figure 7: Optimal flow splits of separators vs inlet flow rate ($\alpha_{in} = 0.4$)

5. Conclusions

The model for deoiler has been fitted to match data for oil concentrations $\alpha_{in} \in [0.1 \text{ } 0.4]$ and for a throughput of $10 \text{ m}^3/\text{h}$. Hence, the model deviates from the experimental results close to the phase inversion point i.e. close to $\alpha_{in} = 0.66$ and for high inlet flow rates. Further experimental work for lower oil cuts will help improve the model. The optimal flow splits have been found to be close to the oil cut in the inlet of the respective separators, as expected.

We gratefully acknowledge good discussions with Sigurd Skogestad at the outset of this work.

References

- S. Balakrishna, L. T. Biegler, 1992. Targeting strategies for the synthesis and energy integration of nonisothermal reactor networks. *Industrial & Engineering Chemistry Research* 31 (9), 2152–2164.
- A. Constantinides, N. Mostoufi, 1999. *Numerical Methods for Chemical Engineers with MATLAB Applications*. Prentice-Hall Inc., Upper Saddle River, New Jersey.
- M. Dirkwanger, 1996. *A New Axial Cyclone Design for Fluid-Fluid Separation*. Ph.D. thesis, Delft University of Technology.
- A. F. Sayda, J. H. Taylor, 2007. Modeling and Control of Three-Phase Gravity Separators in Oil Production Facilities. In: *American Control Conference*. pp. 4847–4853.
- J. J. Slot, 2013. *DEVELOPMENT OF A CENTRIFUGAL IN-LINE SEPARATOR FOR OIL-WATER FLOWS*. Ph.D. thesis, University of Twente.
- L. van Campen, 2014. *Bulk Dynamics of Droplets in Liquid-Liquid Axial Cyclones*. Ph.D. thesis, Delft University of Technology.